Ab initio study of the structure and dynamics of bulk liquid Fe

M. Marqués, L. E. González, and D. J. González
Departamento de Física Teórica, Universidad de Valladolid, 47011 Valladolid, Spain
(Received 23 March 2015; revised manuscript received 12 June 2015; published 5 October 2015)

Several static and dynamic properties of bulk liquid Fe at a thermodynamic state near its triple point have been evaluated by *ab initio* molecular dynamics simulations. The calculated static structure shows very good agreement with the available experimental data, including an asymmetric second peak in the structure factor which underlines a substantial local icosahedral short-range order in the liquid. The dynamical structure reveals propagating density fluctuations, with an associated dispersion relation which closely follows the experimental data. The dynamic structure factors $S(q,\omega)$ show a good agreement with their experimental counterparts which have been recently measured by an inelastic x-ray scattering experiment. The dynamical processes behind the $S(q,\omega)$ have been analyzed by using a model with two decay channels (a fast and a slow) associated with the relaxations of the collective excitations. The recent finding of transverselike excitation modes in the IXS data is analyzed by using the present *ab initio* simulation results. Several transport coefficients have been evaluated and the results are compared with the available experimental data.

DOI: 10.1103/PhysRevB.92.134203 PACS number(s): 61.20.Ja, 61.20.Lc, 62.60.+v

I. INTRODUCTION

For the last two decades or so, the research into the physical properties of iron under extreme conditions has been a field of intense activity, both theoretical and experimental. As the Earth's core is largely composed of iron, an understanding of the different phenomena occurring in the core presumes a knowledge about the behavior of the solid and liquid phases of iron at those pressure and temperature conditions occurring in the core. Moreover, the complexity of laboratory research under those conditions has stimulated a substantial amount of theoretical and molecular dynamics (MD) simulation studies which have addressed a variety of thermodynamical, structural, electronic, and transport properties of solid and liquid iron and some alloys [1–5].

The experimental work has already provided information on several thermodynamic [6–8] and structural [9–13] properties of iron, although most work has focused on crystalline Fe rather than liquid Fe (l-Fe) because of the greater practical complications posed by the liquid phase.

The static structure factor of l-Fe near its triple point has been measured by x-ray diffraction (XD) [9,10] and neutron diffraction (ND) [11] techniques. It displays a symmetric main peak followed by a second maximum with a small shoulder on its right-hand side. This peculiar feature in the second maximum has been found in other transition metals (Ni, Ti, Zr) [11,14] and in liquid Mg [15], and has been related to icosahedral (either ideal or distorted) short-range order that is enhanced upon undercooling [16]. Recently, Shen *et al.* [13] have measured the static structure factor of l-Fe at several pressures up to 58 GPa and temperatures up to 2900 K and they found that, within this pressure/temperature range, the shape of the static structure factor remained qualitatively similar to that at the triple point.

The microscopic dynamics of l-Fe has recently been studied experimentally by Hosokawa *et al.* [17], who have performed inelastic x-ray scattering (IXS) measurements of l-Fe at 1843 K. The dynamic structure factor $S(q,\omega)$ was determined within the range $0.13 \leqslant q \leqslant 2.13\,\text{Å}^{-1}$ and the results were analyzed by modeling the $S(q,\omega)$ in terms of a central Lorentzian function plus a damped harmonic oscillator (DHO) model. Propagating collective excitations were detected and its associated dispersion relation yielded an adiabatic velocity of sound $\approx$3800 m/s. By resorting to the Landau-Placzek relation, the generalized heat capacity ratio $\gamma(q)$ was derived and it was found that for $q \leqslant 1\,\text{Å}^{-1}$ the $\gamma(q)$ slightly diminishes with decreasing q, leading (when $q \to 0$) to a ratio of specific heats of $\approx$1.40. Based on this result, they suggested a qualitative explanation for the appearance of well defined collective excitations in l-Fe. Finally, another striking result was the observation of transverselike excitation modes in their IXS data [18]; more specifically, those modes showed up as shoulders in the measured $S(q,\omega)$ and within a small range of q values.

Prompted by the above experimental data, we have performed a study on several static and dynamic properties of l-Fe near its triple point. We have used an *ab initio* molecular dynamics (AIMD) simulation method which is nowadays a standard technique for the study of a wide range of condensed matter systems. Most AIMD methods are based on density functional theory [19] which, given a number of atoms at given nuclear positions, allows us to compute the ground state electronic energy and the forces acting on the atoms. Then, those forces are used to find the evolution of the system, thereby enabling us to perform MD simulations with the nuclear positions evolving according to classical mechanics, whereas the electronic subsystem follows adiabatically. Although the AIMD methods require significant computational resources and impose important constrains concerning the simulation times and size of the systems under study, nevertheless these drawbacks are compensated by the accuracy of the results yielded.

We recall that AIMD simulations as well as classical MD (CMD) simulations based on empirical potentials have been performed for l-Fe in a wide range of thermodynamic states, although most of them have focused on a range of high pressures and temperatures mimicking those of the Earth's core. Usually those studies have evaluated several thermodynamic and structural properties as well as some transport

coefficients. The first AIMD simulation of l-Fe was carried out by Vocadlo *et al.* [1] and it reported results for the static structure of l-Fe at two temperatures ($T = 6000$ and 4300 K) which were considered representative of those at the inner core and the core-mantle boundary, respectively. Subsequently, other AIMD studies of l-Fe under core conditions have evaluated different static properties [2,3], transport coefficients (self-diffusion and shear viscosity) [2,20], adiabatic sound velocity [21], or the melting curve [22].

Oddly enough, there is only one AIMD simulation study of l-Fe near its triple point [23] and it was just focused on several static properties of liquid and undercooled Fe. The simulation used 100 particles, an ultrasoft pseudopotential, and the generalized gradient approximation (GGA) for the electronic exchange and correlation energy. This study included spin polarization as it was assumed that local magnetic moments exist even above the Curie point; indeed, they found that inclusion of magnetic moments was important in order to correctly describe the short-range order in l-Fe.

However, the dynamical properties of l-Fe (apart from some transport coefficients) have not been studied by means of the AIMD simulation technique yet. Indeed, the only available simulation study of the dynamic properties is a CMD simulation by Bryk and Belonoshko [24]. These authors used an embedded atom model (EAM) effective potential that had been previously constructed by fitting to AIMD calculations at high temperatures, where l-Fe is assumed to be nonmagnetic. Note that this implies that magnetic effects are explicitly excluded in calculations that use this potential. Subsequently they performed CMD simulations employing this EAM potential in order to evaluate several static and dynamic properties of l-Fe near its triple point. The calculated time correlation functions were analyzed within the context of the generalized collective modes (GCM) method, which is a theoretical framework to analyze the hydrodynamic and nonhydrodynamic collective processes existing, with different spatial and time scales, in liquids. However, comparison with experiment was restricted to the values of the sound velocity and the ratio of specific heats at constant pressure and at constant volume.

We stress that none of the theoretical studies near the melting point reported above, be it CMD or AIMD, have considered the dynamic structure factors, which are key magnitudes to describe the dynamic properties of l-Fe, that, as mentioned previously, have been already measured by IXS. *A fortiori*, there has been no previous analysis about the possibility of finding signatures of transverse modes in the dynamic structure factor, as has also been reported experimentally.

We have carried out an AIMD simulation study of several static and dynamic properties of l-Fe at a thermodynamic state near its triple point. Besides its intrinsic interest, we have chosen this specific thermodynamic state because of the recent availability of inelastic x-ray scattering measurements [17]. Our calculations extend the previous AIMD study [23] into the realm of dynamic properties, and also the previous CMD study [24] by analyzing the dynamic structure factors throughout the use of a more accurate approach (DFT vs EAM) that incorporates important aspects of the interactions, including magnetism, which were ignored in such CMD studies.

The layout of the paper is as follows: In Sec. II we briefly present the theory underlying the AIMD simulation method and we describe some technical details as well as some of the terms appearing in the Kohn-Sham energy functional. In Sec. III we report and discuss the obtained structural and dynamical results which are compared with other previous studies as well as with the available experimental data. Finally, some conclusions are drawn.

II. COMPUTATIONAL METHOD

The AIMD simulations have been performed with the VASP code [25]. For each ionic configuration, the Kohn-Sham energy functional is minimized leading to the ground state electronic density. Then the forces on the ions are obtained via the Hellman-Feynman theorem, and the ionic positions and velocities are updated by solving Newton's equations of motions using the velocity Verlet algorithm. The electronic exchange-correlation energy has been described by the Perdew-Burke-Ernzerhof generalized gradient approximation (GGA) [26] and we have used the projector augmented wave (PAW) all-electron description of the electron-ion-core interaction [27]. We used eight valence electrons per atom (s and d), which is enough at this range of pressures, the plane-wave cutoff was set to 300 eV and the electronic iterations converged within 10^{-5} eV. We employed a 120-atom cubic supercell with periodic boundary conditions and fixed periodic lengths to reproduce the experimental ionic number density $\rho = 0.0746\,\text{Å}^{-3}$ at 1873 K. Spin polarization was included with the spin interpolation of the correlation energy proposed by Vosko *et al.* [28] to account for the existence of local magnetic moments above the Curie point. For simulations of this size, a single k point (Γ) was more than adequate for performing accurate reciprocal-space summations. The equilibration process for the initial randomly chosen atomic positions lasted 4 ps and therefrom, microcanonical AIMD simulations were performed over 40 ps with a time step of 2 fs. These latter 20 000 equilibrium configurations were employed for the evaluation of several static and dynamic properties of bulk l-Fe.

Finally, in order to study the influence of the local magnetic moments on the above structural properties, as has been suggested by Ganesh and Widom [23], we have also performed another set of AIMD simulations using 150 atoms and assuming a nonmagnetic (NM) state (i.e., no magnetic moments).

III. RESULTS

A. Static properties

The AIMD simulations provide a direct evaluation of both the pair distribution function $g(r)$ and the static structure factor $S(q)$. In Fig. 1 we have depicted the AIMD result for $g(r)$ along with the corresponding XD and ND experimental data. The AIMD $g(r)$ accurately reproduces the main peak's position at $r_p \approx 2.52$ Å, as well as the phase of the subsequent oscillations; moreover, the amplitude of the oscillations practically coincides with the XD data of Inui *et al.* [10]. Incidentally, we stress that the NM-AIMD calculation gives a $g(r)$ whose main peak is located at a shorter distance, namely $r_p \approx 2.42$ Å,

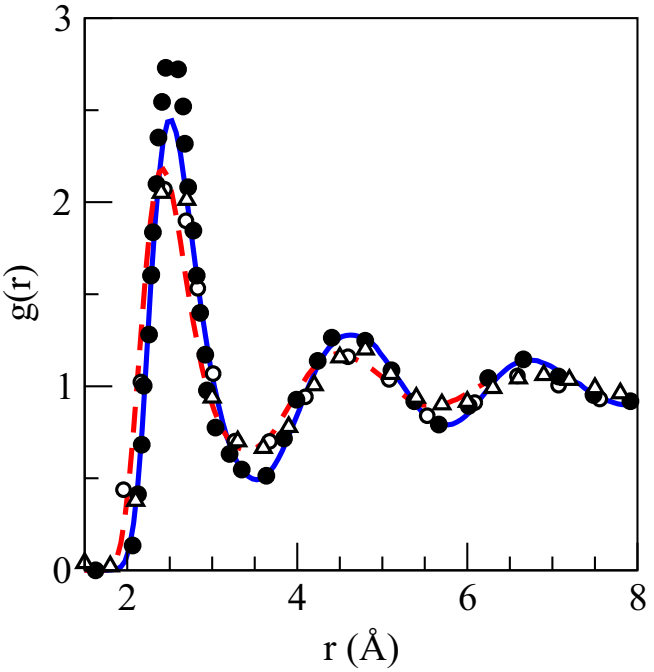

FIG. 1. (Color online) Pair distribution function $g(r)$ of l-Fe. Continuous (broken) line: AIMD (NM-AIMD) calculations for l-Fe at $T = 1873$ K. Open triangles and full circles: experimental XD data at 1843 K from Waseda [9] and Inui [10], respectively. Open circles: experimental ND data at 1873 K from Schenk *et al.* [11].

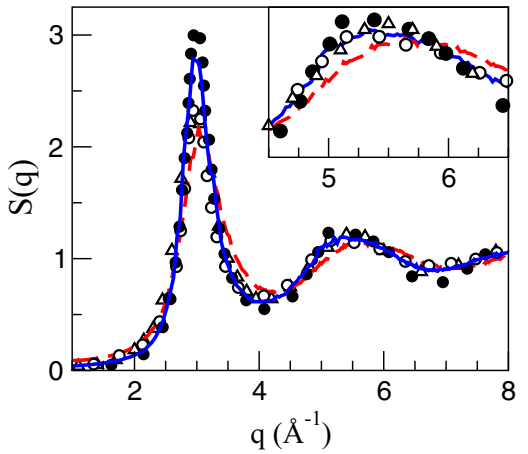

FIG. 2. (Color online) Static structure factor $S(q)$ of liquid Fe. Continuous (broken) line: AIMD (NM-AIMD) calculations for l-Fe at $T = 1873$ K. Open circles: experimental ND data at 1873 K from Schenk *et al.* [11]. Full circles and open triangles: experimental XD data at 1843 K from Inui *et al.* [10] and Waseda [9], respectively. The inset shows a detailed comparison for the second maximum.

and the ensuing oscillations are somewhat out of phase with respect to the experimental data.

The coordination number (CN) has been evaluated by integrating the radial distribution function $4\pi\rho r^2 g(r)$ up to the position of its first minimum, which for the AIMD $g(r)$ is located at $R_{\min} = 3.42$ Å, leading to a value CN ≈ 12.5 atoms. Had we chosen to integrate up to $r_{\min} = 3.52$ Å, which is the position for the first minimum in $g(r)$, then CN ≈ 13.1 atoms. These values for CN are typical of the simple liquid metals around their respective triple point [29]. We stress that these structural results are very similar to those obtained in the AIMD simulation study of Ganesh and Widom [23].

Figure 2 shows the AIMD result for $S(q)$, which is compared with the experimental ND [11] and XD [9,10] data. The experimental $S(q)$'s have a symmetric main peak located at a position $q_p \approx 2.98$ Å^{-1} and its height varies between $S(q_p) \approx 2.3$ of Waseda [9] and ≈3.0 of Inui *et al.* [10]. Moreover, both the XD [10] and the ND data [11] show a shoulder in the second maximum at $q \approx 6.0$ Å^{-1}. The AIMD result for $S(q)$ stands in a very good agreement with the experimental data, i.e., its main peak's position is at $q_p \approx 2.99$ Å^{-1} and its height is $S(q_p) \approx 2.8$, whereas the subsequent oscillations are in phase with experimental data; more remarkably, its second maximum displays a small shoulder at $q \approx 6.0$ Å^{-1}. It is worth noting that an asymmetric shape of the second peak of $S(q)$ has been experimentally observed in several other liquid metals and it has been related to a significant presence of icosahedral local order. A first indication of such type of short-range order is given by the positions of the maximum of the second peak of $S(q)$, q_2, and its shoulder q_2', as compared to the position of the main peak. The values found for l-Fe in this study are $q_2/q_p = 1.79$ and $q_2'/q_p \approx 1.91$, which are similar to those found for l-Ti and l-Zr (1.76 and 1.92), for l-Ni (1.74 and 1.95), and for liquid Mg and other alkaline-earth metals [30] (1.80 and 1.97); else they are comparable to those corresponding to an ideal icosahedral environment in a curved space [31], namely 1.71 and 2.04.

On the other hand, the NM-AIMD simulations produce an $S(q)$ whose main peak is slightly displaced towards greater q values, i.e., $q_p \approx 3.05$ Å^{-1}, and its height is lower than the experimental data; moreover, as evidenced by the inset of Fig. 2, the subsequent oscillations are somewhat displaced towards greater q values.

We have also estimated the isothermal compressibility κ_T of l-Fe by resorting to the equation $S(q \to 0) = \rho k_B T \kappa_T$, where k_B is Boltzmann's constant. First, the low q values of $S(q)$ were extrapolated to $q \to 0$ by using a least squares fit $S(q) = s_0 + s_2 q^2$ of the calculated q values for $q \leqslant 1.2$ Å^{-1}. We obtained an estimate $S(q \to 0) = 0.024 \pm 0.002$, yielding a value $\kappa_T = 1.24 \pm 0.10$ (in units of 10^{-11} m^2 N^{-1}) which is close to the experimental data $\kappa_T \approx 1.21 \pm 0.02$ [32]. Again we note that an equivalent calculation using the NM-AIMD result for $S(q)$ produced a result $S(q \to 0) = 0.20 \pm 0.02$, and a value $\kappa_T = 10.3 \pm 0.2$.

A more detailed description of the local order in the liquid can be achieved by resorting to the common neighbor analysis [33] (CNA) method. Here each pair of atoms is characterized by four indices, with the first index being 1 if the pair belongs to the first peak of $g(r)$. The second index is the number of common first neighbors and the third index is the number of bonds that connect those shared first neighbors. Finally, the fourth index is used to distinguish configurations with the same first three indices but with a different topology. The CNA method allows us to discern fcc, hcp, bcc, and icosahedral (ICOS) packings as well as

TABLE I. Common neighbor analysis of the AIMD configurations of l-Fe at 1873 K compared with several local structures.

Pairs	l-Fe	NM l-Fe	ICOS	hcp	fcc	bcc
1551	0.35	0.17	1.00	0.00	0.00	0.00
1541	0.18	0.16	0.00	0.00	0.00	0.00
1431	0.17	0.23	0.00	0.00	0.00	0.00
1321	0.02	0.09	0.00	0.00	0.00	0.00
1421	0.02	0.03	0.00	0.50	1.00	0.00
1422	0.03	0.07	0.00	0.50	0.00	0.00
1441	0.08	0.04	0.00	0.00	0.00	0.43
1661	0.13	0.04	0.00	0.00	0.00	0.57

more complex polytetrahedral environments. For example, fcc and hcp crystalline packings are composed of 142×-type pairs, bcc is typified by 144× and 166× pairs, whereas ICOS is characterized by 155× pairs and the distorted ICOS is described by the 154× and 143× pairs. We have taken several configurations generated in the present AIMD simulation, found the corresponding inherent structures (local minimum of the energy surface closest to the selected configuration) by removing the thermal energy, and finally we have performed a CNA analysis of the inherent structures. After averaging over the configurations, we have obtained the results summarized in Table I.

First, notice that the fivefold symmetry dominates in l-Fe as the sum of perfect and defective icosahedral structures amounts to 72% of the pairs (65% of the pairs in the NM-AIMD calculation), with the number of perfect ones being nearly half of the total. Moreover, we also find a 21% appearance of local bcc environments, which is the phase in which l-Fe crystallizes. These results are similar to those already obtained in the AIMD simulations of Ganesh and Widom [23]; moreover, their calculation for undercooled l-Fe showed an increase in the percentage of 1551 pairs. Furthermore, the ND data of Schenk *et al.* [11] for undercooled l-Fe display a shoulder on the second maximum of $S(q)$ which becomes more noticeable with decreasing temperature. All in all, these features point to a high ability of l-Fe for undercooling, which agrees with a similar behavior found in other liquid transition metals [11,16].

B. Dynamic properties

Several dynamic properties, both single-particle ones (velocity autocorrelation function, mean square displacement) and collective ones (intermediate scattering functions, dynamic structure factors, longitudinal and transverse currents) have also been evaluated. We note that the calculation of the time correlation functions was performed by taking time origins every five time steps. Some correlation functions have a dependence on the wave vector $\vec{q}$ which, for an isotropic system, reduces to a dependence on $q \equiv |\vec{q}|$ only.

1. Single particle dynamics

Information about transport properties can be extracted from the normalized velocity autocorrelation function of a tagged ion in the fluid $Z(t)$, which is defined as

$$Z(t) = \langle \vec{v}_1(t) \cdot \vec{v}_1(0) \rangle / \langle v_1^2 \rangle, \quad (1)$$

with $\vec{v}_1(t)$ being the velocity of a tagged ion in the fluid at time t and $\langle \cdots \rangle$ standing for the ensemble average. The calculated $Z(t)$, which is depicted in Fig. 3, displays the typical backscattering behavior with a marked first minimum which is followed by rather weak oscillations. This first minimum is related to the so-called cage effect by which a given particle rebounds against the cage formed by its nearest neighbors. An estimate of the frequency at which a given particle vibrates within its near neighbor's cage [34] can be derived by the short time expansion $Z(t) = 1 - \omega_E^2 t^2/2 \cdots$, where ω_E is the so-called "Einstein frequency" of the system. A short time fitting of the calculated $Z(t)$ curve in Fig. 3 gives $\omega_E \approx 32.4$ ps^{-1}. The inset of Fig. 3 represents the associated power spectrum $Z(\omega)$, which shows a maximum located at ≈25 ps^{-1} and a shoulder at ≈39 ps^{-1}; parenthetically we note that ω_E stands between the peak and the shoulder of $Z(\omega)$, which is a characteristic feature of the simple liquid metals [29]. On the other hand, the NM-AIMD simulation yields a much weaker cage effect.

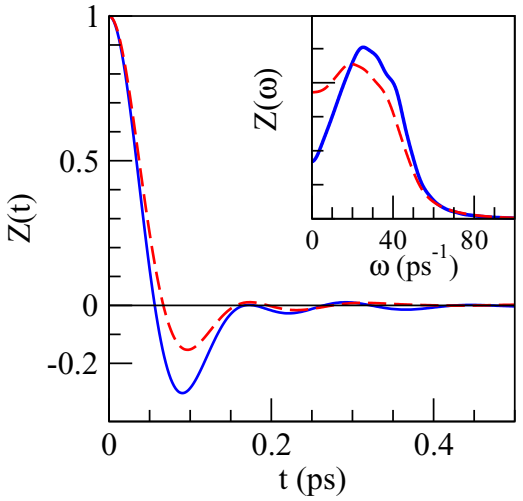

FIG. 3. (Color online) Normalized AIMD calculated velocity autocorrelation function of liquid Fe at 1873 K (full line). The inset represents its power spectrum $Z(\omega)$. The dashed lines stand for the NM-AIMD calculation.

The self-diffusion coefficient D can be found by either the time integral of $Z(t)$ or from the slope of the mean square displacement $\delta R^2(t) \equiv \langle |\vec{R}_1(t) - \vec{R}_1(0)|^2 \rangle$ of a tagged ion in the fluid. In this AIMD study, both routes yield the same value, namely $D_{\mathrm{AIMD}} = 0.37 \pm 0.02$ Å^2/ps at $T = 1873$ K, which is comparable to other estimates, i.e., the CMD calculation of Belashchenko [35] gave $D \approx 0.368$ Å^2/ps for l-Fe at $T = 1820$ K, whereas the AIMD simulations of Sobolev *et al.* [36] for l-Fe at $T = 1833$ K gave $D = 0.350$ Å^2/ps. Moreover, by using experimental data for other thermodynamic magnitudes, Iida *et al.* [37] have suggested a value $D_{\mathrm{exp}} \approx 0.355$ Å^2/ps for l-Fe at $T = 1811$ K. Finally, we mention that the NM-AIMD calculation gives a substantially greater value, namely $D = 0.82 \pm 0.03$ Å^2/ps at $T = 1873$ K.

2. *Collective dynamics*

The intermediate scattering function $F(q,t)$ is defined as

$$F(q,t) = \frac{1}{N}\left\langle \left(\sum_{j=1}^{N} e^{-i\vec{q}\vec{R}_j(t+t_0)}\right)\left(\sum_{l=1}^{N} e^{i\vec{q}\vec{R}_l(t_0)}\right)\right\rangle \quad (2)$$

and it contains information on the collective dynamics of density fluctuations. Its frequency spectrum is the dynamic structure factor $S(q,\omega)$, which can be directly measured by either inelastic neutron scattering (INS) or inelastic x-ray scattering (IXS) experiments. Another relevant quantity, which is also connected to the density fluctuations, is the current due to the overall motion of the particles $\vec{j}(q,t)$ defined as

$$\vec{j}(q,t) = \sum_{a=1}^{N} \vec{v}_a(t)\ \exp[i\vec{q}\cdot\vec{R}_a(t)], \quad (3)$$

which is usually split into a longitudinal component $\vec{j}_L(q,t)$, parallel to $\vec{q}$, and a transverse component $\vec{j}_T(q,t)$, perpendicular to $\vec{q}$. The longitudinal and transverse current correlation functions are obtained as

$$C_l(q,t) = \frac{1}{N}\langle j_L(q,t) j_L^*(q,0)\rangle \quad (4)$$

and

$$C_t(q,t) = \frac{1}{2N}\langle \vec{j}_T(q,t)\cdot\vec{j}_T^*(q,0)\rangle. \quad (5)$$

The respective time Fourier transforms (FT) give the associated spectra $C_l(q,\omega)$ and $C_t(q,\omega)$. The previous dynamical magnitudes have been calculated from the configurations generated in the present AIMD simulations. Moreover, in order to analyze the microscopic mechanisms ruling the collective dynamics, we have performed a detailed theoretical analysis of the $F(q,t)$ by resorting to the generalized Langevin formalism (see the Appendixes for details). Thus, using the AIMD results for the $F(q,t)$ we have calculated its first- and second-order memory functions $M(q,t)$ and $N(q,t)$, respectively; subsequently the $N(q,t)$ has been fitted to an analytical model containing two exponentially decaying functions (a slow and a fast one), i.e.,

$$N(q,t) = A_s(q)e^{-t/\tau_s(q)} + A_f(q)e^{-t/\tau_f(q)}, \quad (6)$$

where $\tau_s(q)$ and $\tau_f(q)$ are the slow and fast relaxation times. Physically, one relaxation channel is considered of thermal origin, whereas the other is related to the viscoelastic behavior of the liquid. The model allows two possible physical interpretations for the terms in $N(q,t)$. One choice identifies the thermal relaxation with the slow channel, whereas the viscoelastic relaxation is described by the fast one. The other choice, which implies making the reverse identifications, has been suggested by Scopigno *et al.* [38] as a result of their analysis of experimental IXS data for liquid Li. More details about this model are given in the Appendixes.

Figure 4 shows some AIMD simulation $F(q,t)$, for several q values. The $F(q,t)$ exhibit an oscillatory behavior up to $q \approx (4/5)q_p$, with the amplitude of the oscillations becoming weaker for increasing q values; moreover, this oscillatory shape is superposed on a rather weak diffusive component. At $q \approx q_p$, the $F(q,t)$ exhibit a slow decay, known as "de

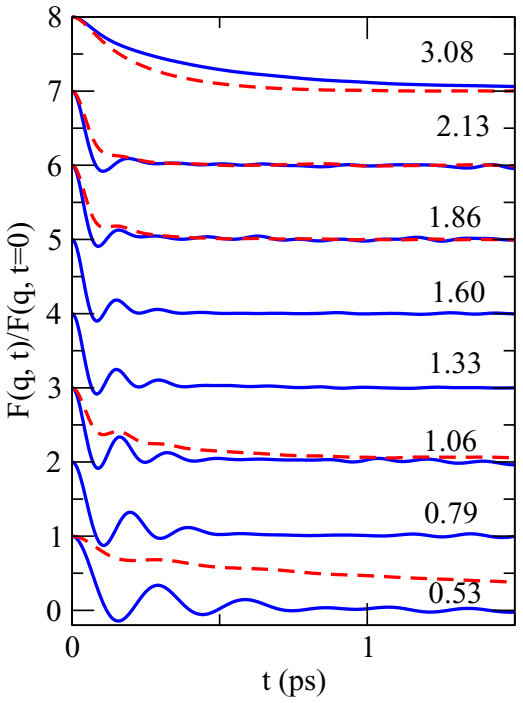

FIG. 4. (Color online) Normalized AIMD intermediate scattering functions $F(q,t)$ at several q values (in Å^{-1} units), for liquid Fe at $T = 1873$ K (full lines). The vertical scales are offset for clarity. The dashed lines are the NM-AIMD results.

Gennes narrowing," which is induced by the strong spatial correlations at around those q values. Remarkably, we note that a similar qualitative behavior, including the marked oscillations at small q values, is also displayed by the $F(q,t)$ obtained in the CMD simulations and GCM calculations of Bryk and Belonoshko [24] for l-Fe. Indeed, a very similar trend is found in the simple liquid metals near their respective triple point [39–43].

In Fig. 4 we have also plotted the NM-AIMD results for the $F(q,t)$, which are qualitatively different from the previous ones; now the $F(q,t)$ are dominated by a strong diffusive component, which is superposed, up to $q \approx (4/5)\,q_p$, on a very weak oscillatory behavior.

Using the previous AIMD results for $F(q,t)$, we have determined their respective second-order memory functions $N(q,t)$. Figure 5 shows, for some q values, the obtained $N(q,t)$ as well as its two components, namely, its fast and slow decay channels. At the smaller $q = 0.54\,\text{Å}^{-1}$, both channels contribute in the time range below $\approx$10 fs, although for shorter times the fast channel has a contribution around twice that of the slow one. With increasing q values, the contribution of the fast channel at short times becomes more important and its rule over the memory function extends to a longer time range; in fact for $q = 2.0\,\text{Å}^{-1}$, the fast channel dominates up to times $\approx$100 fs.

Next, we analyze the physical origin of both relaxation channels in order to find out whether the present AIMD results for the $N(q,t)$ are consistent with a generalized hydrodynamic model (fast viscoelastic channel and a slow thermal one), or a generalized viscoelastic model, where the fast term is the

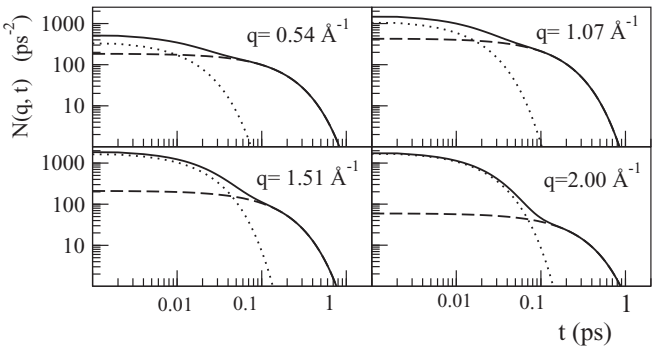

FIG. 5. Memory function $N(q,t)$ for several q values (full line) along with its two exponential components. The dashed line represents the slow component and the dotted line stands for the fast component.

thermal one. Therefore, we have evaluated the generalized heat capacity ratio $\gamma(q)$, which in the $q \to 0$ limit leads to the thermophysical value of γ_0, i.e., the ratio between specific heats at constant pressure and at constant volume (see the Appendixes). The obtained results for $\gamma(q)$ are dependent on the model used. If the thermal relaxation proceeds on the slow channel, then $A_s(q) = [\gamma(q) - 1]M_0(q)$ and $\tau_s(q) = [\gamma(q)D_T(q)]^{-1}$. But if the viscoelastic relaxation occurs along the slow channel then $A_s(q) = \omega_L^2(q) - \gamma(q)M_0(q)$. Therefore, using the $A_s(q)$ values calculated in the evaluation of the $N(q,t)$, we have derived the functions $\gamma_{\rm th}(q)$ and $\gamma_v(q)$ which correspond to the thermal and the viscoelastic relaxations along the slow channel, respectively. The results are depicted in Fig. 6 along with the "experimental" $\gamma_{\rm expt}(q)$ data of Hosokawa *et al.* [17].

We already mentioned that $\gamma_{\rm expt}(q)$ was estimated by fitting the experimental $S(q,\omega)$ to an analytical model and subsequently applying the Landau-Placzek relation. Although some uncertainty is bound to this procedure, as for example in the observed data scattering for $q \leqslant 0.70\,\text{Å}^{-1}$, however we believe that the qualitative trend is correct, namely that for

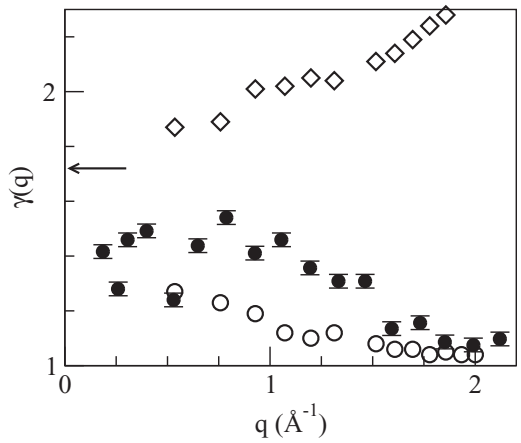

FIG. 6. Generalized specific heat ratio $\gamma(q)$ as obtained from either the generalized hydrodynamic model (circles) or the generalized viscoelastic model (lozenges). The full circles with error bars are experimental IXS data of Hosokawa *et al.* [17]. The arrow shows the hydrodynamic value $\gamma_0 \approx 1.72$.

$q \geqslant 1.0\,\text{Å}^{-1}$, the $\gamma_{\rm expt}(q)$ rapidly decreases with increasing q and it goes to one at $q \approx q_p/2$. Indeed, a similar trend has been obtained in theoretical calculations of $\gamma(q)$ for liquid Li, Bi, Pb, Hg, and Cd [44,45]. As for the present calculations, we observe that the $\gamma_v(q)$ takes greater values than the experiment and quickly increases with q. On the other hand, the $\gamma_{\rm th}(q)$ qualitatively follows the experimental results and it appears to smoothly approach a $q \to 0$ value similar to that of the experimental $\gamma_{\rm expt}(q)$. In our opinion, this result clearly suggests that the slow channel is the one through which the thermal relaxation takes place and that the generalized hydrodynamic model is the appropriate one for describing the microscopic dynamics of l-Fe near the triple point.

The model of Eq. (6) leads to an associated $F(q,t)$ with an analytical expression comprising four exponential terms (two real and two with complex conjugate amplitudes and exponents), i.e.,

$$\frac{F(q,t)}{S(q)} = A_1 \exp(-a_1 t) + A_2 \exp(-a_2 t) + \exp(-bt)[B\cos(\omega_s t) + C\sin(\omega_s t)]. \quad (7)$$

Out of the eight q-dependent parameters only four are left as independent when the correct short time behavior (initial value equal to one, zero initial values for the first and third derivatives, and initial value of the second derivative equal to the second frequency moment) is imposed.

This model provides a very good description of the AIMD simulation results for the $F(q,t)$, and it could be useful in order to obtain an analytic expression of $S(q,\omega)$ as a sum of two central Lorentzians plus a pair of stretched Lorentzian inelastic peaks. It would be especially interesting if the raw calculated $F(q,t)$ displayed relatively large noise for long times due to the limited statistics. In fact, the present calculations do not show such a problem and the results presented below for $S(q,\omega)$ are obtained by numerical Fourier transformation of the AIMD $F(q,t)$, after application of a window function (see the Appendixes for details).

A proper comparison with the IXS data requires a convolution of the AIMD calculated $S(q,\omega)$ with the experimental resolution function [17] as well as the inclusion of the detailed balance factor [29]. Now the $S(q,\omega)$ thus obtained are plotted, for several q values, in Figs. 7 and 8 where they are compared with the IXS data of Hosokawa *et al.* [17]. Up to $q \approx (4/5)q_p$ we observe side peaks which are indicative of collective density excitations and for greater q's the $S(q,\omega)$ show a monotonic decreasing behavior. In general, the AIMD calculated $S(q,\omega)$ qualitatively agree with experiment, specially concerning the position and amplitude of the side peaks.

From the positions of the side peaks $\omega_m(q)$, the corresponding dispersion relation of the density fluctuations has been derived and its slope at $q \to 0$ yields the adiabatic sound velocity c_s. Unfortunately, the small size of the simulation box implies that the smallest attainable q value is $q_{\rm min} = 0.536\,\text{Å}^{-1}$, which is not small enough to afford a precise quantitative estimate of c_s; nevertheless a qualitative guess may be extracted from the value of $\omega_m(q_{\rm min})$ which leads to $c_{s,\rm AIMD}(q_{\rm min}) \approx 3950 \pm 150$ m/s. An additional check on

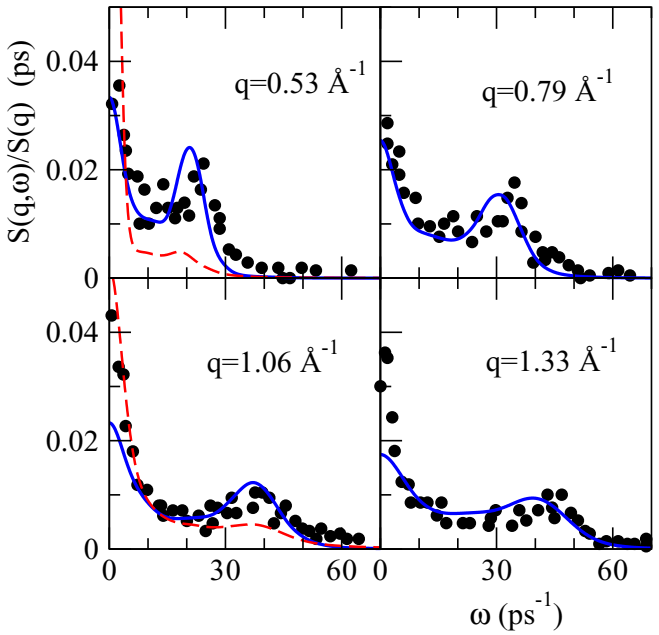

FIG. 7. (Color online) Dynamic structure factors $S(q,\omega)$ of liquid Fe at several q values. Full circles: experimental IXS data at $T = 1843$ K [17]. Full (dashed) line: present AIMD (NM-AIMD) results after convolution with the experimental resolution function.

this estimate can be made by resorting to the expression [34] $c_s = [\gamma k_B T/mS(q \to 0)]^{1/2}$, where m is the atomic mass. Using for the ratio of the specific heats $\gamma \approx 1.40$ [24] and our calculated value $S(q \to 0) = 0.024$, the previous expression gives $c_s = 4030 \pm 250$ m/s, which attests to the consistency between the static and dynamic results obtained in the present AIMD study. For comparison we recall that the experimental hydrodynamic value is $c_{s,\text{expt}} \approx 3820 \pm 150$ m/s [7].

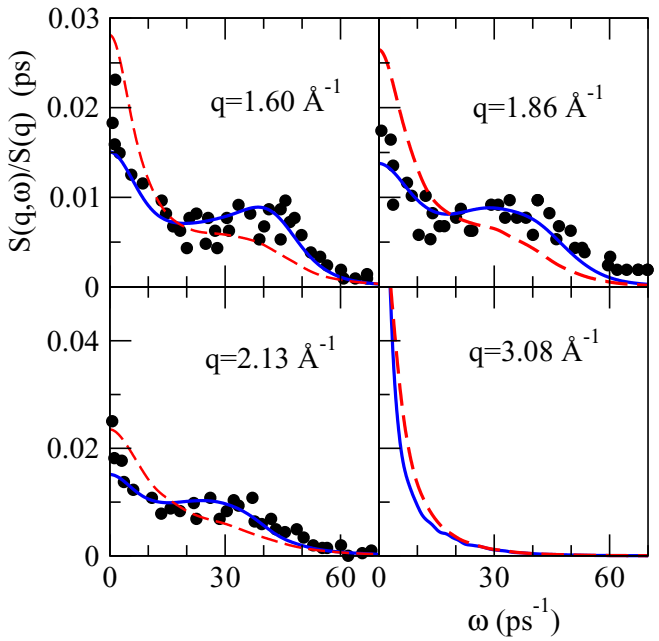

FIG. 8. (Color online) Same as in the previous figure.

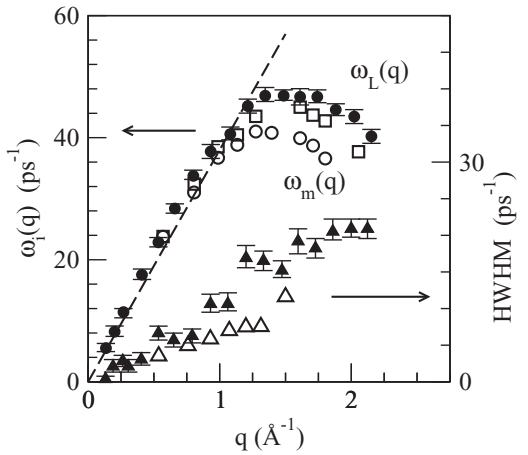

FIG. 9. Dispersion relation for l-Fe at $T = 1873$ K. Open circles and squares: AIMD results from the positions of the inelastic peaks in the $S(q,\omega)$ and from the maxima in the spectra of the longitudinal current $C_l(q,\omega)$, respectively. Full circles with error bars: IXS data from Hosokawa *et al.* [17]. Broken line: linear dispersion with the hydrodynamic sound velocity $c_s = 3820$ m/s. Full (open) triangles with error bars: experimental (calculated) values for the HWHM $\Gamma(q)$ of the inelastic peaks.

We have also included in Fig. 9 the dispersion relation $\omega_l(q)$, which is calculated from the maxima of the AIMD results for $C_l(q,\omega)$. Moreover, the figure also includes the experimental dispersion $\omega_l(q)$ data of Hosokawa *et al.* [17]. According to these authors, the experimental dispersion relation data exhibit, in the low-q region, a positive dispersion, i.e., an increase of the $\omega_l(q)$ values with respect to those given by the linear dispersion of the experimental adiabatic sound velocity. A similar conclusion has also been drawn from the CMD simulations and the subsequent GCM analysis of Bryk and Belonoshko [24]. Although it appears that the AIMD results for both $\omega_m(q)$ and $\omega_l(q)$ may suggest some kind of positive dispersion, however, the scarcity of small q values afforded by the present AIMD simulations prevents us from ascertaining the appearance of positive dispersion.

Another magnitude related to the collective density excitations is the half-width at half-maximum (HWHM) $\Gamma(q)$ of the inelastic peaks because it provides information on the lifetimes of the excitations. This magnitude cannot be obtained solely from the values of $S(q,\omega)$, since it is necessary to single out the contribution from the propagating excitations to the dynamic structure factor. This can only be accomplished by using a model. For this purpose only we have fitted our $F(q,t)$ to Eq. (7), and identified the parameter b with $\Gamma(q)$. The experimental data [17] for $\Gamma(q)$ (which were also obtained via a model for the dynamic structure factor) show an almost linear behavior up to $q \approx q_p/2$, which suggests that the hydrodynamic limit (quadratic law) is restricted to very low q values. This is depicted in Fig. 9 along with our calculated $\Gamma(q)$.

In Figs. 7 and 8 we have also depicted, for several q values, the dynamic structure factors derived from the NM-AIMD simulations (after convolution with the experimental resolution function [17] and the inclusion of the detailed balance factor). Again we observe side peaks at approximately

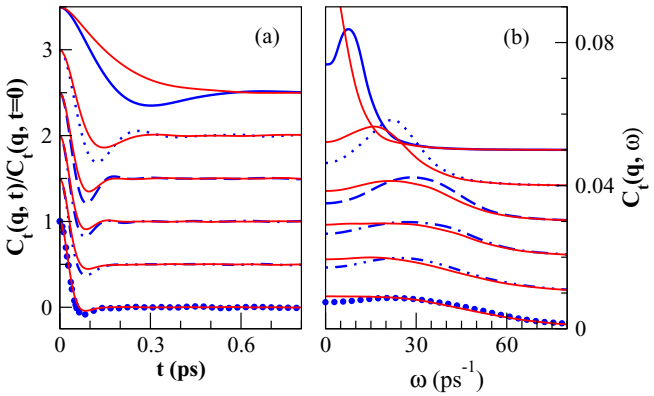

FIG. 10. (Color online) (a) Transverse current correlation function $C_t(q,t)$ at several q values for liquid Fe at $T = 1873$ K and $q = 0.54\,\text{Å}^{-1}$ (full curve), $q = 1.20\,\text{Å}^{-1}$ (dotted curve), $q = 2.00\,\text{Å}^{-1}$ (dashed curve), $q = 3.08\,\text{Å}^{-1}$ (dashed-dotted curve), $q = 4.05\,\text{Å}^{-1}$ (dashed-double dot curve), and $q = 5.03\,\text{Å}^{-1}$ (full circles). The vertical scales are offset for clarity. (b) Same for the spectra $C_t(q,\omega)$. The light red curves are the results of the NM-AIMD simulations.

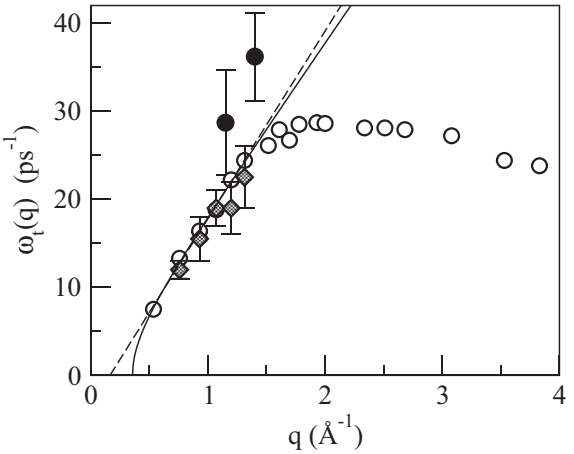

FIG. 11. Transverse dispersion relation for liquid Fe at $T = 1873$ K. Open circles: AIMD results from the positions of the peaks in the spectra $C_t(q,\omega)$. Full line: fit to the nonanalytic viscoelastic expression. Dashed line: linear fit. The lozenges with error bars (full circles with error bars) are the positions of the transverselike inelastic modes in the calculated (experimental) dynamic structure factors $S(q,\omega)$.

the same positions as the previous calculations but their amplitudes are markedly smaller than the experimental ones; moreover, those side peaks appear in a narrower q range, i.e., up to $q \approx (3/5)q_p$.

The transverse current correlation function $C_t(q,t)$ is not directly measurable, but provides valuable information related to the existence of shear modes. Its spectrum $C_t(q,\omega)$, when plotted as a function of ω, may display peaks within some q range, which are related to propagating shear waves. This is shown in Fig. 10 which depicts the AIMD results for $C_t(q,t)$ and $C_t(q,\omega)$. The latter has been obtained by numerical FT after application of a window function, the same procedure as used for $F(q,t)$. The $C_t(q,\omega)$ already shows a peak at the smallest available q, i.e., $q_{\min} = 0.18q_p$ and those peaks appear up to $q \leqslant 2.5q_p$; moreover, its frequency increases with q, reaches a maximum value at $q \approx q_p$, and then slowly decreases until the peaks eventually disappear. In fact, this behavior is comparable to what has been found in the simple liquid metals [29].

From the position of the maximum in the $C_t(q,\omega)$, a dispersion relation for the transverse modes $\omega_t(q)$ has been obtained and this is plotted in Fig. 11. The existence of a propagation gap in the shear waves means that the dispersion starts at a q_t (to be estimated later), smoothly increases up to $(3/5)q_p$, and therefore has a quasiflat behavior. Indeed the present AIMD result resembles that obtained by the GCM method of Bryk and Belonoshko [24].

The general behavior of the transverse dispersion relation, at least in the vicinity of the wave vector region where shear waves start being supported by the system, is well described by a viscoelastic model [29,30], which leads to a nonanalytic behavior $\omega_t^v(q) = \alpha\sqrt{q^2 - q_t^2}$. A fit of the previously obtained data to such an expression (with parameters α and q_t) provides a value of $q_t \approx 0.36\,\text{Å}^{-1}$, as shown in Fig. 11. However, the behavior of $\omega_t(q)$ near q_t is in fact almost linear (except very close to q_t) and the slope of this line, which is close to the group velocity of the shear waves in this wave vector region, can be identified with a velocity of transverse waves $c_t \approx 2200$ m/s, near the onset of their appearance.

From the AIMD results for the $C_t(q,t)$, the associated shear viscosity coefficient η can be derived [39,46]; thus we have obtained an estimate $\eta_{\text{AIMD}} = 5.0 \pm 0.3$ GPa ps. For comparison the experimental value for l-Fe at melting ($T = 1809$ K) is $\eta = 5.82$ GPa ps [47], but its extrapolation to $T = 1873$ K gives $\eta_{\text{expt}} \approx 5.30$ GPa ps. On the other hand, based on a critical analysis of different experimental data, Assael *et al.* [48] have suggested a value of $\eta_{\text{expt}} \approx 5.20 \pm 0.05$ GPa ps for l-Fe at $T = 1873$ K. Finally, we notice that the NM-AIMD calculations yield an estimate $\eta = 1.8 \pm 0.2$ GPa ps which grossly underestimates the experimental value.

Within the context of the Brownian motion of a macroscopic particle with a diameter d in a liquid of viscosity η, the Stokes-Einstein (SE) relation $\eta D = k_B T/2\pi d$ establishes a connection between η and the self-diffusion coefficient D. Although not intended for atoms, this relation has been used to estimate η (or D) by identifying d with the position of the main peak of $g(r)$. The present calculations give $d = 2.52$ Å, and when combined with the previous AIMD value $D_{\text{AIMD}} = 0.37 \pm 0.02\,\text{Å}^2/\text{ps}$ yields an estimate $\eta = 4.40 \pm 0.3$ GPa ps which is slightly smaller, by ≈15%, than the calculated AIMD value. Indeed, a similar degree of accuracy has been found in the application of the SE relation to a variety of liquid metals near melting. On the other hand, most studies on l-Fe at high pressure and temperature conditions have relied on the SE relation in order to evaluate the shear viscosity in terms of a calculated self-diffusion coefficient, and therefore the degree of accuracy of such relation should be kept in mind for a critical analysis.

Recently it has been suggested [49] that transverselike low-energy excitations may be observed as weak shoulders located between the quasielastic peak and the longitudinal inelastic peak of the dynamic structure factors. Moreover,

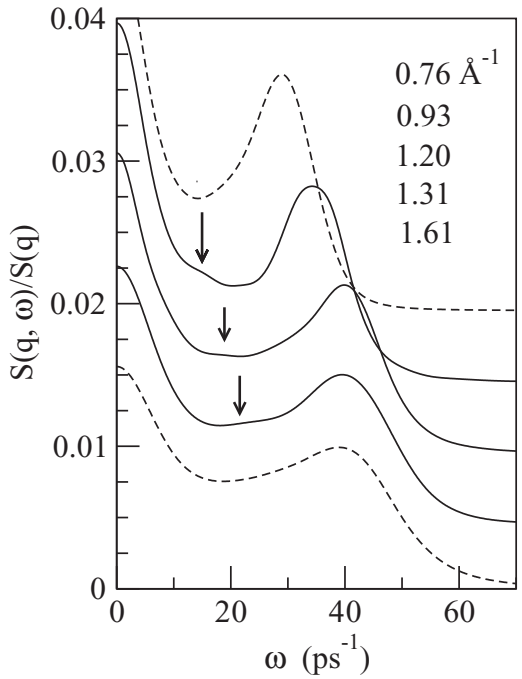

FIG. 12. AIMD calculated dynamic structure factors $S(q,\omega)/S(q)$ for (top to bottom) $q = 0.76$, 0.93, 120, 1.31, and 1.61 Å^{-1}. The vertical scales are offset for clarity. The arrows point to the locations of the transverselike excitations at $q = 0.93$, 1.20, and 1.31 Å^{-1}.

those excitations should show up within a small q range located around $q_p/2$, because for smaller q values those transverselike excitation modes are either overcome by the quasielastic peak or quickly decrease in intensity. These transverselike excitations were first detected in the IXS spectra of l-Ga [49] at 313 K; and subsequently have also been observed in l-Cu, l-Sn, and l-Fe [18,50]. In the specific case of l-Fe at $T = 1823$ K, the IXS data [18] for $S(q \approx 1.20,\omega)$ point to a transverselike excitation located at $\omega \approx 25.0\,\text{ps}^{-1}$. Therefore, we have analyzed the present AIMD results for $S(q,\omega)$ and the results are plotted in Fig. 12. It is observed that within the range $0.90 \leqslant q \leqslant 1.40$ Å^{-1}, weak shoulders appear in the region between the quasielastic and the inelastic peaks; moreover, the shoulder in the $S(q = 1.20,\omega)$ is located at $\omega \approx 20.0$ ps^{-1}. On the other hand, no shoulders or similar features are visible in the $S(q,\omega)$ corresponding to $q \leqslant 0.76$ and $q \geqslant 1.61$ Å^{-1}. Additionally, in Fig. 11 we have plotted the frequencies associated with these shoulders and it can be observed that they practically agree with the peak positions of the transverse current spectra. We consider these results as another strong indication concerning its interpretation as transverselike excitation modes.

IV. CONCLUSIONS

We have reported an *ab initio* simulation study on the dynamical properties of l-Fe at a thermodynamic state near its triple point. This study has been spurred by the recent inelastic x-ray scattering measurements of Hosokawa *et al.* [17].

A range of static properties have also been evaluated. Thus, results have been presented for the pair distribution function $g(r)$ and the static structure factor $S(q)$; both magnitudes show a very good agreement with the available experimental data [9–11]. Moreover, the obtained results for $S(q)$ show an asymmetric shape in its the second peak. This has been connected to the appearance of icosahedral short-range order, which has been confirmed by a more detailed CNA study of the liquid structure.

As for the dynamic structure, the calculated intermediate scattering functions $F(q,t)$ have been used to analyze the role of the different decay channels associated with the relaxations of the collective excitations. Its second-order memory function was evaluated and fitted to a sum of two exponentially decaying functions describing a fast and a slow relaxation processes. The ensuing discussion about the physical origin of both relaxation processes, which was based on the evaluation of the generalized $\gamma(q)$, suggests that a generalized hydrodynamic model is adequate for describing the microscopic dynamics of l-Fe near the triple point. The calculated dynamic structure factors show side peaks, within some q range, which are indicative of collective density excitations; moreover they exhibit a good agreement with the IXS data. The calculated dispersion relation closely follows the experimental data. Furthermore, we stress that closer analysis of the obtained $S(q,\omega)$ has unveiled the same type of transverselike excitation modes as found by Hosokawa *et al.* [18] in their IXS data.

The AIMD transverse current correlation functions $C_t(q,t)$ exhibit clear oscillations around zero and the associated spectra $C_t(q,\omega)$ have inelastic peaks which reflect the presence of shear waves in l-Fe. The calculated transport coefficients, namely self-diffusion and shear viscosity, show a good agreement with the experimental data. We have also examined the reliability of the Stokes-Einstein relation because it has been widely used to evaluate the shear viscosity of l-Fe at high pressure and temperature conditions, and found that it underestimates the viscosity by around 15%.

In the previous AIMD simulations of Ganesh and Widom [23], it was already shown that for a good description of the static structure of liquid Fe it was necessary to take into account the existence of atomic magnetic moments, through the use of spin-polarized DFT. We have found in our study that dynamic properties are even more sensitive to the inclusion of these atomic magnetic moments, as some magnitudes are way off the experimental ones if nonspin-polarized calculations are performed, e.g., the diffusion constant is overestimated by more than 100% and correspondingly the shear viscosity is grossly underestimated.

Obviously the magnetic properties of liquid Fe are poorly described by the AIMD method used here: the simulated system has a spontaneous magnetic moment which cannot be present in real liquid Fe. There are however several indications, both experimental [51] and theoretical [52,53], that suggest that liquid Fe is paramagnetic, so that atomic magnetic moments are indeed present in the system, although there is no long-range magnetic order. The average atomic magnetic moment obtained in our simulations is 2.41 Bohr magnetons. On the other hand, the excellent agreement between the experimental static structure and dynamic properties and the

simulated ones suggests that the interatomic forces are well reproduced by the theoretical method used.

We conclude that it is essential to take into account the existence of atomic magnetic moments in order to describe the interactions among atoms, even though the magnetic ordering is exacerbated and leads to wrong magnetic properties. While it might happen that a more detailed account of magnetism, considering, e.g., the possibility of noncollinearity, could alleviate the inaccuracies observed, we nevertheless consider that this exacerbation of magnetic ordering is an intrinsic defect of DFT in the study of finite temperature magnetism. In fact, there have been theoretical constructs, like the dynamic mean field theory [52], that take into account correlation effects, absent in DFT, that kill off ferromagnetism and produce a paramagnetic behavior of solid bcc-Fe above a Curie temperature. This temperature is usually largely overestimated, but further improvements in the theory [53] can lead to values comparable to the experimental Curie temperature. However, such methods have only been applied to solids, where the symmetries reduce the number of nonequivalent atoms to a very small number. It seems very unlikely that this kind of more exact methods (with respect to magnetism) will become applicable to liquid systems, with at least one hundred atoms needed in order to take into account structural and dynamic disorder.

ACKNOWLEDGMENTS

We warmly thank Professor A. Vega for enlightening discussions on theoretical approaches to the calculation of magnetic properties at nonzero temperature. M.M. acknowledges the financial support of the Universidad de Valladolid and Junta de Castilla y León (CIP13/03). L.E.G. and D.J.G. acknowledge the support of the Ministerio de Ciencia e Innovación (FIS2014-59279-P) and Junta de Castilla y León (VA104A11-2).

APPENDIX A: MODEL FOR $N(q,t)$

We start by introducing the hierarchy of memory functions of $F(q,t)$ and this is most conveniently achieved through the use of the Laplace transform technique $\tilde{f}(z) = \int_0^\infty f(t)\exp[-zt]dt$. In this way the first $M(q,t)$ and second-order $N(q,t)$ memory functions of $F(q,t)$ are defined as

$$\tilde{F}(q,z) = \frac{F_0(q)}{z + \tilde{M}(q,z)}, \quad \tilde{M}(q,z) = \frac{M_0(q)}{z + \tilde{N}(q,z)}, \tag{A1}$$

where $F_0(q)$ and $M_0(q)$ are the initial ($t = 0$) values of $F(q,t)$ and $M(q,t)$, respectively, and take the values $F_0(q) = S(q)$ and $M_0(q) = -\ddot{F}(q,0)/F_0(q) = k_B T q^2/[mS(q)]$ the dot denoting time derivative, with k_B the Boltzmann constant and m the atomic mass. Moreover, since $F(q,t)$ is a real even function of time, its second derivative can be related to the second frequency moment of the $S(q,\omega)$, so that $M_0(q) = \langle\omega^2(q)\rangle/S(q) = \int_{-\infty}^{\infty} \omega^2 S(q,\omega)/S(q)\, d\omega$.

The second-order memory function $N(q,t)$ accounts for all the relaxation processes in the collective dynamics and is a basic magnitude in most theoretical models for $F(q,t)$. Usually the $N(q,t)$ has been written as a sum of a rapidly decaying term, which aims to describe the interactions of a particle with its nearest neighbors, plus a slowly decaying term intending to account for the cooperative motion of a large number of particles. A convenient mathematical description is achieved by writing the $N(q,t)$ as a sum of two exponentially decaying functions (a slow and a fast one), namely

$$\begin{aligned} N(q,t) &= A_s(q)e^{-t/\tau_s(q)} + A_f(q)e^{-t/\tau_f(q)}, \\ \tilde{N}(q,z) &= \frac{A_s(q)}{z + \tau_s(q)^{-1}} + \frac{A_f(q)}{z + \tau_f(q)^{-1}}. \end{aligned} \tag{A2}$$

This model [54] conventionally ascribes to one of the exponentials the physical origin of a thermal decay channel, with amplitude $[\gamma(q) - 1]M_0(q)$ and relaxation time $[\gamma(q)D_T(q)]^{-1}$, whereas the other exponential accounts for a viscoelastic decay channel, with amplitude $\omega_L^2(q) - \gamma(q)M_0(q)$ and relaxation time $\tau_v(q)$. The values of the amplitudes are such that $N(q,t = 0)$ recovers its correct value in terms of the second and fourth derivatives of $F(q,t)$ at $t = 0$ or alternatively in terms of the second and fourth frequency moments of $S(q,\omega)$, where in particular $\omega_L^2(q) = \langle\omega^4(q)\rangle/\langle\omega^2(q)\rangle$. The other q-dependent magnitudes, namely $\gamma(q)$ and $D_T(q)$, are generalizations of the thermophysical parameters $\gamma_0 = C_P/C_V$ (the ratio between specific heats at constant pressure and at constant volume) and the thermal diffusivity D_T. We end up by remarking that the analytical properties of the exponential functions are suitable for the fitting of simulation data for $F(q,t)$; in fact the previous model leads to an $F(q,t)$ with an analytical expression comprising four exponential terms (two real and two with complex conjugate amplitudes and exponents).

APPENDIX B: WINDOW FOR FOURIER TRANSFORMS

The Fourier transform of a function of time $F(t)$ into frequency space $\tilde{F}(\omega)$ involves an integral over all times from 0 to infinity. In time correlation functions it is unavoidable to have some small, but unphysical, statistical noise at long times. This can lead to erroneous results in the FT, and the usual prescription to eliminate this source of errors is the multiplication, prior to the integration, of the raw function $F(t)$ by a window function $W(t)$ that starts from one and goes smoothly to zero for long times. In particular, the window we use is defined as

$$W(t) = \begin{cases} 1, & 0 \leqslant t \leqslant t_0 \\ \exp[-(t - t_0)^2/\tau^2], & t \geqslant t_0. \end{cases}$$

We have chosen this form in order to preserve the initial time derivatives of $F(t)$, which are related to the frequency moments of $\tilde{F}(\omega)$.

[1] L. Vocadlo, G. A. de Wijs, G. Kresse, M. Gillan, and G. D. Price, Faraday Discuss. **106**, 205 (1997).

[2] D. Alfe, G. Kresse, and M. J. Gillan, Phys. Rev. B **61**, 132 (2000).

[3] L. Vocadlo, D. Alfe, M. J. Gillan, and G. D. Price, Phys. Earth Planet. Int. **140**, 101 (2003); M. J. Gillan, D. Alfe, J. Brodholt, L. Vocadlo, and G. D. Price, Rep. Prog. Phys. **69**, 2365 (2006).

[4] Z.-Y. Zeng, C.-E Hu, X.-R. Chen, L.-C. Cai, and F.-Q. Jing, J. Phys. Condens. Matter **20**, 425217 (2008); D. Alfe, Phys. Rev. B **79**, 060101 (2009); Yu. D. Fomin, V. N. Ryzhov, and V. V. Brazhkin, J. Phys. Condens. Matter **25**, 285104 (2013).

[5] A. B. Belonoshko, S. Arapan, and A. Rosengren, J. Phys. Condens. Matter **23**, 485402 (2011).

[6] W. W. Anderson and T. J. Ahrens, J. Geophys. Res. **99**, 4273 (1994).

[7] P. M. Nasch, M. H. Manghnani, and R. A. Secco, J. Geophys. Res. **99**, 4285 (1994).

[8] M. D. Rutter, R. A. Secco, H. Liu, T. Uchida, M. L. Rivers, S. R. Sutton, and Y. Wang, Phys. Rev. B **66**, 060102(R) (2002); R. A. Secco, M. D. Rutter, S. P. Balog, H. Liu, D. C. Rubie, T. Uchida, D. Frost, Y. Wang, M. L. Rivers, and S. R. Sutton, J. Phys. Condens. Matter **14**, 11325 (2002); D. P. Dobson, Phys. Earth Planet. Int. **130**, 271 (2002); L. S. Dubrovinsky, S. K. Saxena, F. Tutti, S. Rekhi, and T. LeBehan, Phys. Rev. Lett. **84**, 1720 (2000).

[9] Y. Waseda, *The Structure of Non-Crystalline Materials* (McGraw-Hill, New York, 1980).

[10] M. Inui, K. Maruyama, Y. Kajihara, and M. Nakada, Phys. Rev. B **80**, 180201 (2009).

[11] T. Schenk, D. Holland-Moritz, V. Simonet, R. Bellissent, and D. M. Herlach, Phys. Rev. Lett. **89**, 075507 (2002).

[12] C. Sanloup, F. Guyot, P. Gillet, G. Fiquet, R. Hemley, M. Mezouar, and I. Martinez, Europhys. Lett. **52**, 151 (2000).

[13] G. Shen, V. B. Prakapenka, M. L. Rivers, and S. R. Sutton, Phys. Rev. Lett. **92**, 185701 (2004).

[14] G. W. Lee, A. K. Gangopadhyay, R. W. Hyers, T. J. Rathz, J. R. Rogers, D. S. Robinson, A. I. Goldman, and K. F. Kelton, Phys. Rev. B **77**, 184102 (2008).

[15] S. Tahara, H. Fujii, Y. Yokota, Y. Kawakita, S. Kohara, and S. Takeda, Physica B **385-386**, 219 (2006).

[16] T. H. Kim and K. F. Kelton, J. Chem. Phys. **126**, 054513 (2007); N. Jakse and A. Pasturel, Phys. Rev. Lett. **91**, 195501 (2003); J. Chem. Phys. **120**, 6124 (2004); N. Jakse, O. Le Bacq, and A. Pasturel, J. Non-Crystal. Solids **353**, 3684 (2007).

[17] S. Hosokawa, M. Inui, K. Matsuda, D. Ishikawa, and A. Q. R. Baron, Phys. Rev. B **77**, 174203 (2008).

[18] S. Hosokawa, S. Munejiri, M. Inui, Y. Kajihara, W.-C. Pilgrim, A. Q. R. Baron, F. Shimojo, and K. Hoshino, AIP Conf. Proc. **1518**, 695 (2013); S. Hosokawa, M. Inui, S. Tsutsui, and A. Q. R. Baron, J. Phys. Condens. Matter **27**, 194104 (2015).

[19] P. Hohenberg and W. Kohn, Phys. Rev. **136**, B864 (1964); W. Kohn and L. J. Sham, *ibid.* **140**, A1133 (1965).

[20] G. A. de Wijs, G. Kresse, L. Vocadlo, D. Dobson, D. Alfe, M. J. Gillan, and G. D. Price, Nature (London) **392**, 805 (1998).

[21] D. Alfe, G. D. Price, and M. J. Gillan, Phys. Rev. B **65**, 165118 (2002).

[22] D. Alfe, G. D. Price, and M. J. Gillan, J. Phys. Chem. Solids **65**, 1573 (2004).

[23] P. Ganesh and M. Widom, Phys. Rev. B **77**, 014205 (2008).

[24] T. Bryk and A. B. Belonoshko, Phys. Rev. B **86**, 024202 (2012).

[25] G. Kresse and J. Hafner, Phys. Rev. B **47**, 558(R) (1993); **49**, 14251 (1994); G. Kresse and J. Furthmuller, Comput. Mater. Sci. **6**, 15 (1996); Phys. Rev. B **54**, 11169 (1996).

[26] J. P. Perdew, K. Burke, and M. Ernzerhof, Phys. Rev. Lett. **77**, 3865 (1996).

[27] P. E. Blochl, Phys. Rev. B **50**, 17953 (1994); G. Kresse and D. Joubert, *ibid.* **59**, 1758 (1999).

[28] S. H. Vosko, L. Wilk, and M. Nusair, Can. J. Phys. **58**, 1200 (1980).

[29] U. Balucani and M. Zoppi, *Dynamics of the Liquid State* (Clarendon, Oxford, 1994).

[30] B. G. del Rio and L. E. Gonzalez, J. Phys. Condens. Matter **26**, 465102 (2014).

[31] S. Sachdev and D. R. Nelson, Phys. Rev. Lett. **53**, 1947 (1984).

[32] R. S. Hixson, M. A. Winkler, and M. L. Hodgdon, Phys. Rev. B **42**, 6485 (1990).

[33] J. D. Honeycutt and H. C. Andersen, J. Phys. Chem. **91**, 4950 (1987).

[34] J. P. Hansen and I. R. McDonald, *Theory of Simple Liquids* (Academic, London, 1986); J. P. Boon and S. Yip, *Molecular Hydrodynamics* (Dover, New York, 1991).

[35] D. Belashchenko, Russ. J. Phys. Chem. **80**, 758 (2006).

[36] A. Sobolev and A. Mirzoev, J. Mol. Liquids **179**, 12 (2013).

[37] T. Iida, R. I. L. Guthrie, and N. Tripathi, Metal. Mater. Trans. B **37**, 559 (2006).

[38] T. Scopigno, U. Balucani, G. Ruocco, and F. Sette, J. Phys. Condens. Matter **12**, 8009 (2000).

[39] D. J. González, L. E. González, J. M. López, and M. J. Stott, Phys. Rev. B **65**, 184201 (2002); J. Chem. Phys. **115**, 2373 (2001).

[40] A. Torcini, U. Balucani, P. H. K. de Jong, and P. Verkerk, Phys. Rev. E **51**, 3126 (1995); M. M. G. Alemany, L. J. Gallego, and D. J. González, Phys. Rev. B **70**, 134206 (2004); M. M. G. Alemany, R. C. Longo, L. J. Gallego, D. J. González, L. E. González, M. L. Tiago, and J. R. Chelikowsky, *ibid.* **76**, 214203 (2007).

[41] F. Shimojo, K. Hoshino, and M. Watabe, J. Phys. Soc. Jpn. **63**, 141 (1994); S. Sengul, L. E. González, and D. J. González, J. Phys. Condens. Matter **21**, 115106 (2009).

[42] S. Kambayashi and G. Kahl, Phys. Rev. A **46**, 3255 (1992); G. Kahl and S. Kambayashi, J. Phys. Condens. Matter **6**, 10897 (1994).

[43] L. E. González, D. J. González, and M. Canales, Z. Phys. B **100**, 601 (1996); J. Casas, D. J. González, L. E. González, M. M. G. Alemany, and L. J. Gallego, Phys. Rev. B **62**, 12095 (2000); L. Calderín, D. J. González, L. E. González, and J. M. López, J. Chem. Phys. **129**, 194506 (2008).

[44] M. Canales, L. E. González, and J. A. Padró, Phys. Rev. E **50**, 3656 (1994); T. Bryk and I. Mryglod, J. Phys. Condens. Matter **12**, 3543 (2000); **13**, 1343 (2001); Phys. Rev. E **63**, 051202 (2001).

[45] L. Calderín, L. E. González, and D. J. González, J. Chem. Phys. **130**, 194505 (2009); J. Phys. Condens. Matter **23**, 375105 (2011); **25**, 065102 (2013).

[46] U. Balucani, J. P. Brodholt, P. Jedlovszky, and R. Vallauri, Phys. Rev. E **62**, 2971 (2000); J. Blanco, D. J. González, L. E. González, J. M. López, and M. J. Stott, *ibid.* **67**, 041204 (2003); L. E. González and D. J. González, Phys. Rev. B **77**, 064202 (2008).

[47] M. Shimoji and T. Itami, *Atomic Transport in Liquid Metals* (Trans. Tech. Publications, Switzerland, 1986).

[48] M. J. Assael, K. Kakosimos, R. M. Banish, J. Brillo, I. Egry, R. Brooks, P. N. Quested, K. C. Mills, A. Nagashima, Y. Sato, and W. A. Wakeham, J. Phys. Chem. Ref. Data **35**, 285 (2006).

[49] S. Hosokawa, M. Inui, Y. Kajihara, K. Matsuda, T. Ichitsubo, W.-C. Pilgrim, H. Sinn, L. E. González, D. J. González, S. Tsutsui, and A. Q. R. Baron, Phys. Rev. Lett. **102**, 105502 (2009); Eur. Phys. J. Special Topics **196**, 85 (2011).

[50] S. Hosokawa, S. Munejiri, M. Inui, Y. Kajihara, W.-C. Pilgrim, Y. Ohmasa, T. Sutsui, A. Q. R. Baron, F. Shimojo, and K. Hoshino, J. Phys. Condens. Matter **25**, 112101 (2013).

[51] Y. Waseda and K. Suzuki, Phys. Status Solidi B **39**, 669 (1970).

[52] A. I. Lichtenstein, M. I. Katsnelson, and G. Kotliar, Phys. Rev. Lett. **87**, 067205 (2001).

[53] V. I. Anisimov, A. S. Belozerov, A. I. Poteryaev, and I. Leonov, Phys. Rev. B **86**, 035152 (2012).

[54] U. Bafile, E. Guarini, and F. Barocchi, Phys. Rev. E **73**, 061203 (2006).